Check for updates

Method for the use of polymer beads as dosimeters for low-energy electron irradiation

Joana Kira Besecke[1,2,3], Lysann Kenner[1], André Poremba[1], Jessy Schönfelder[4,5], Tobias Teichmann[1], Martin Thoma[3,6], Thomas Grunwald[3,7], Elizabeth von Hauff[1,8], Ulla König[1], Björn Poppe[2] and Simone Schopf[1,3]*[†]

[1]Customized Electron Beam Systems and Technologies, Fraunhofer Institute for Electron Beam and Plasma Technology (FEP), Dresden, Germany, [2]Division Medical radiation physics, Carl von Ossietzky University of Oldenburg, Oldenburg, Germany, [3]Fraunhofer Cluster of Excellence Immune-Mediated Diseases CIMD, Frankfurt am Main, Germany, [4]Elektronenstrahlprozesse, Fraunhofer Institute for Electron Beam and Plasma Technology (FEP), Dresden, Germany, [5]Diagnostics department, Fraunhofer Institute for Cell Therapy and Immunology (IZI), Leipzig, Germany, [6]Pharmaceutical and Bioproduction Technology, Fraunhofer Institute for Manufacturing Engineering and Automation (IPA), Stuttgart, Germany, [7]Department for Vaccines and Infection Models, Fraunhofer Institute for Cell Therapy and Immunology (IZI), Leipzig, Germany, [8]Faculty of Electrical and Computer Engineering, Technical University Dresden, Dresden, Saxony, Germany

In this study, a novel bead-based dosimetry system was developed. This approach uses suspended polymethyl methacrylate beads, which experience a dose-dependent change in fluorescence intensities. The beads were diluted in deionized water and exposed to low-energy electron irradiation. Afterward, the beads were analyzed by flow cytometry. The mean fluorescence of these beads increased with the radiation dose in the range of 10−50 kGy. Thus, flow cytometric fluorescence measurements allow dose mapping: the signal of each bead could be assigned to a corresponding dose. The correlation between the dose and fluorescence intensity of the beads was previously examined by irradiation using a high-energy electron beam. The presented method shows potential for dosimetry in liquids for quality control in biotechnological or pharmaceutical applications using low-energy electron irradiation as the method is easy to handle, not limited to solid-state geometry, and suitable for static and dynamic irradiation setups of liquids. This novel method provides information about the dose distribution in the investigated volume of liquid by analyzing individual beads. This provides information about average, minimum, and maximum dose values, as well their actual distribution function, which is a big advantage over other methods of liquid dosimetry, where only the mean value can be obtained.

KEYWORDS

dosimetry, liquid dosimeters, fluorescence, beads, low-energy electron irradiation, process monitoring

1 Introduction

Low-energy electron irradiation (LEEI) involves the use of electrons with energies below 300 keV. This technology is characterized by high dose rates, low thermal effects, and low production of bremsstrahlung [1]. Thus, LEEI is a powerful tool for medical and biotechnological applications. Recent studies have shown that LEEI can effectively inactivate pathogens in liquid solution. For instance, viruses such as the influenza A virus,

Zika virus, and respiratory syncytial virus can be inactivated by LEEI at 20–25 kGy while maintaining their structure [2–4]. Furthermore, bacteria such as *Escherichia coli* were inactivated at a dose of 2.5 kGy. In addition, LEEI has the potential to inactivate cells to produce immunotherapeutics [5]. A disadvantage of LEEI is the steep dose gradient in the irradiated material as the absorbed dose decreases rapidly with the penetration depth. Due to this factor, a fixed sample is not irradiated uniformly [6], and dosimetry is challenging.

Dosimeters are mandatory to monitor whether samples are receiving the required dose. Various dosimeters are available in the form of solid, liquid, and gas detectors. Solid-state dosimeters include radiochromic films and alanine films or tablets, which change their radical concentration, or electrical, such as semiconductor chips and metal–oxide–semiconductor field-effect transistors [7, 8]. However, this study focuses on liquid dosimetry systems. LEEI of liquids requires additional considerations compared to dosimetry for solids because liquids exhibit flow behavior. The development of liquid dosimeters is still a research topic. To date, the gold standard for liquid dosimeters is the Fricke solution, which is based on radiation-induced oxidation of ferrous ions to ferric ions but is limited to a maximum dose value of 400 Gy [9]. Although many liquid dosimeters are radiochromic, another example of a liquid dosimeter is scintillation detectors. Scintillation detectors consist of organic or inorganic scintillation materials, such as crystals or plastics, which are dissolved in a liquid, and a photodetector, for instance, a photomultiplier [10]. A disadvantage of such instruments is their high cost.

Another type of dosimeter that changes its optical properties in response to radiation exposure is luminescent dosimeters. Three categories of luminescent dosimeters exist: optically stimulated luminescence dosimeters, thermally stimulated luminescence dosimeters, and radio photoluminescence dosimeters [11]. Optically stimulated and thermally stimulated luminescence dosimeters are primarily storage phosphors, in which radiation induces a latent signal first. Some of the absorbed energy stored in a metastable state can be released in the form of a luminescence signal either by heating or optical stimulation. These related categories are often made of the same luminescent materials but differ in their excitation source and readout technique [12, 13]. Although the luminescence intensity in thermally stimulated and optically stimulated dosimeters decreases as a function of temperature or time of optical stimulation, radio photoluminescence dosimeters display a permanent signal after irradiation [12]. Advantages of radio photoluminescence dosimeters are the small fading effect at room temperature, reusability, good dose linearity, and high reproducibility [14, 15]. Some well-known radio photoluminescence dosimeters are dosimeter badges, including films, glass dosimeters, and especially silver-doped glass dosimeters. Others are fluorescence nuclear track detectors for high-energy particle tracking, which are mainly in a single-crystal form such as aluminum oxide doped with carbon and magnesium or lithium fluoride. Many doped phosphates play a major role in radio photoluminescence dosimetry, such as materials doped with samarium, silver-doped phosphate glasses, materials doped with europium, or calcium fluoride [11]. Commercially available are glass dosimeters relying on radio photoluminescence, which are typically made of silver-activated phosphate glasses and are useful for lower doses below 500 Gy and down to 10 µ Gy [13]. A common dosimeter is the FD7 glass rod

with uncertainties regarding the reading process of 5% (1 *σ*), which can measure up to 1,000 Gy [16]. Furthermore, glass beads with thermoluminescent response with excellent reproducibility below 1% and uncertainties of about 5% were reported in the literature [17, 18]. However, those dosimeters were up to 3 mm in size and tested in the low-dose range below 25 Gy using high-energy photons and gamma rays [17, 18]. New radio photoluminescence materials based on metal–organic frameworks are found in the research for a dose range of 0.1 Gy–3.6 kGy [14].

Finally, dosimetry systems that can measure the dose distribution of liquid setups exposed to low-energy electron beams at the high-dose range are limited. Moreover, current standard dosimeters provide an accumulated dose over the exposed path length, while the dose distribution within a medium remains unknown. Thus, it has not been possible to measure the maximum and minimum absorbed dose and the dose distribution within liquids. This is of interest for the mentioned pharmaceutical applications and the scope of this study.

We describe a method that is based on dose-dependent fluorescence signals occurring from suspended beads in water. These beads allow the dose determination in multiple layers of the liquid, rather than just an average across the entire thickness of the liquid. The spherical beads were detected by flow cytometry. The novelty of this method is this flow-type dosimetry system, which is particularly suitable for dosimetry of small liquid films or fluids irradiated with low-energy electron irradiation. Flow cytometers can measure fluorescence intensities of many small particles (0.5–100 µm) in short time. Liquid samples were collected in a stream traveling beside a laser source, which can excite the particles. Thereby, fluorescence intensities at different wavelengths can be detected in different channels. Furthermore, the scattering properties of the particles can be measured as an indirect unit of size and granularity. Flow cytometric software provides statistical evaluation and visualization of the results in dot plots and histograms. Another benefit is the differentiation by gating the signals in the scattering dot plots as it ensures the measurement of the fluorescence signals of the particles of interest and distinguishes those from other populations or unwanted content, such as dust or deformed particles. Thereby, we measured the fluorescence for each bead individually in gates. After irradiation, we reported a linear gain in fluorescence over a dose range of 10–50 kGy. This method provided information on the relative dose distribution in any static and dynamic irradiation instruments for liquids.

2 Materials and equipment

In this study, different bead dilutions, three different irradiation instruments, and irradiation setups were used, which are discussed in this section. The materials are given in Table 1, 2.

2.1 Choice of material

In this study, polymethyl methacrylate (PMMA) beads were used because such polymer beads are commercially available in many shapes and sizes, ranging from microspheres in the nanoscale to hundreds of micrometers. Beads of polymers such as polymethyl

TABLE 1 List of materials and equipment.

Name	Manufacturer (city, country)	Specification
BD Calibrite Beads (non-labeled)	BD Biosciences (Heidelberg, Germany)	Polymethyl methacrylate Beads (ø 6 µm) 1.5–2.5 E7 beads/mL in Stabilized, buffered saline With 0.1% sodium azide
PMMA-F-KM596	microParticles GmbH (Berlin, Germany)	Polymethyl methacrylate Beads (ø 6 µm) In water (10% solid)
105 00 005	PolyAn GmbH (Berlin, Germany)	Polymethyl methacrylate Beads (ø 5 µm) In water (5% solid)

TABLE 2 List of materials and equipment.

Equipment	Manufacturer/facility	Specification
Irradiation instrument		
ELV-2 (high-energy electron beam)	Budker Institute of Nuclear Physics (Novosibirsk, Russia)	Energy: 0.6–1.5 MeV $I_{max} < 4$ mA
ELLI300 (low-energy electron beam)	Fraunhofer Institute for Electronics, Electron Beam, and Plasma Technology, FEP, (Dresden, Germany)	COMET EBA 300/270 $U_{max} = 300$ kV Target material: copper and titanium
REAMODE (low-energy electron beam)	Fraunhofer Institute for Electron Beam and Plasma Technology, FEP (Dresden, Germany)	LINAC $U_{max} = 200$ kV Copper and titanium Exit window
Irradiation setup		
Petri dishes	Corning® Primaria™ (New York, United States)	Easy grip style Cell culture dish ø = 100 mm
OPP foil	CASFIL (Aves, Portugal)	RINCEL® Coextruded Bi-oriented polypropylene Film (BOPP) ø = 50 mm, t = 48 µm
Microfluidic chip	Fraunhofer Institute for Manufacturing, Engineering, and Automation IPA (Stuttgart, Germany)	25-µm titanium foil
Reference dosimeters		
Crosslinking	Crosslinking AB (Halmstad, Sweden)	Pararosaniline cyanide Dissolved in polyvinyl Butyral Thickness = 10 µm/20 µm Dose range = 5–75 kGy
2,3,5-Triphenyltetrazolium	Carl Roth	$C_{19}H_{15}ClN_4$
Risø B3 film dosimeter	Risø HDRL (Roskilde, Denmark)	Pararosaniline cyanide Dissolved in polyvinyl Butyral Thickness = 18 µm Dose range = 5–100 kGy
Analysis		
FACS Accuri	BD Biosciences (California, United States)	$\lambda_{ex} = 488/640 nm$ Standard filters: 533 nm, 585 nm 610 nm, 670 nm

methacrylate are commonly used for quality tests of flow cytometers and available as transparent unlabeled beads, functionalized beads, and labeled beads, so they are well-suited for flow cytometry. Due to the low density of polymethyl methacrylate (1.2 g/cm³), the material has higher penetration depths for a 200-keV electron beam than for other materials such as glass (2.635 g/cm³) or lithium fluoride (2.635 g/cm³), which was simulated by the eSTAR program (stopping-power and range tables for electrons) at the website of the National Institute of Standards and Technology. Considering the density of the materials and the continuous slowing down approximation (CSDA) range of the 200-keV electron beam, the penetration depth of PMMA was estimated to be 387.4 µm, while

those in glass and lithium fluoride were 229.3 μm and 210.8 μm, respectively (see Supplementary Material S3). In addition, previous tests have shown that the distribution of small polymer beads in water was sufficient, and the risk of sedimentation was less likely than in more dense materials, such as ceramics. This aspect was of importance for the handling during the process in the microfluidic setup.

2.2 Dilution of Becton Dickinson calibrite beads

In this study, unlabeled PMMA beads with a diameter of 6 μm from the Becton Dickinson (BD) Calibrite™ 2-Beads Kit (Becton, Dickinson and Company, Heidelberg, Germany) were used. The beads were suspended in stabilized dilution buffer containing 0.1% sodium azide (BD Calibrite). One bottle of the Calibrite™ 2-Beads Kit contains 2.7 mL bead suspension with $1.5 \cdot 10^7 - 2.5 \cdot 10^7$ of unstained beads per milliliter. The kit also provides different bead suspensions labeled with fluorescence markers: fluorescein isothiocyanate (FITC) and phycoerythrin (PE). However, these beads were not used as previous tests showed that the labels were not stable under irradiation.

For initial high-energy experiments, two drops of bead suspension (approximately 40 μL) were added to 2 mL of the flow solution for fluorescence-activated cell sorting (FACS). The beads were gently vortexed, stored in the refrigerator, and protected from direct sunlight, as recommended in the instructions for use.

To reduce costs and improve the efficiency of the dosimetry system, the bead suspensions were further diluted in deionized water. Previous experiments have shown that the highest feasible dilution is 1:200 (v:v, bead suspension to deionized water), which corresponds to an average bead count of $7 \cdot 10^4$ per mL on average. For the experiments at low-energy electron irradiation, equipment ELLI300 (300 keV) using a microfluidic setup a dilution of 1:50 (v:v, bead suspension to deionized water) with approximately $2.8 \cdot 10^5$ per mL on average was prepared. Here, 1 mL of the BD bead suspensions was approximately 117 €. The beads were stored for 1 day in a refrigerator at approximately 4°C and transported for 2–3 h at room temperature, protected from light, prior to the irradiation experiment.

2.3 Dilution of other polymer beads

For a comparable study, beads made of polymethyl methacrylate purchased from other manufacturers were studied as well: microspheres of 6-μm diameter (microParticles GmbH, Berlin, Germany) in the aqueous solution with a solid content of 10% and microspheres of 5-μm diameter in the aqueous solution with a solid content of 5% (PolyAn GmbH, Berlin, Germany). In order to obtain counts of beads comparable to the previous beads, those beads were diluted with concentrations of 1:10,268 and 1:9,600 (v:v, bead suspension to deionized water). The costs of the beads used for this experiment were approximately 35 € for the beads from microParticles GmbH and 20 € for the beads from PolyAn GmbH. These costs refer to 1 mL each,

which was used for this experiment. One package was purchased for 350 € and 200 €, which is enough for 10 experiments each.

2.4 High-energy electron irradiation equipment for calibration

To assign the fluorescence signals of the polymer beads to certain dose values, the bead suspensions were irradiated using a high-energy electron beam (1.5 MeV). Compared to LEEI, high-energy electron irradiation ensures a more homogeneous dose distribution with a minor dose gradient [19]. Therefore, the dose can be assigned to the fluorescence response. In this experiment, the high-energy irradiator ELV-2 at the Leibniz Institute of Polymer Research Dresden was used.

A static setup of Petri dishes (ø 100 mm) was used, where the dilutions were covered with round foils of orientated polypropylene (OPP), each with a diameter of 50 mm and a thickness of 48 μm. This resulted in a thin liquid film of less than 30 μm. These Petri dishes were covered with a plastic bag (approximately 88 g/m²).

An integrating radiochromic film dosimeter (Crosslinking AB Halmstad, Sweden) was used to measure the reference dose.

2.5 Low-energy electron irradiation equipment for cumulative irradiation

In order to test whether the beads were dependent on the absorbed dose or on other effects, such as dose rate, the bead suspensions (1:2) were irradiated using the LEEI instrument REAMODE (200 keV).

The liquid samples were irradiated in a small-scale setup using Petri dishes [6].
The dose was measured using the reference film dosimeter Risø B3 (DTU Health Tech, Denmark).

2.6 Low-energy electron irradiation equipment for the evaluation of dose distribution

The bead suspensions (1:200) were irradiated in a custom-built LEEI instrument (ELLI300) located at the Fraunhofer Institute for Cell Therapy and Immunology (IZI) in Leipzig, which was designed for the electron beam treatment of liquids at energies up to 300 keV.

The highly diluted bead suspensions were transported through a microfluidic chip, designed by the Fraunhofer Institute for Manufacturing Engineering and Automation (IPA). The chip had eight parallel channels and was covered with a 25-μm titanium foil, which was placed at a distance of 45 mm under the electron exit window [20].

The mean dose to the processed liquid was determined in a previous experiment using a liquid dosimeter based on 2,3,5-triphenyltetrazolium chloride, as described by [3, 6]. This liquid dosimeter was subjected to a radiation-induced reaction with formazan, characterized by a red coloration of the solution and an increase in the absorbance peak at 485 nm. Previous experiments

have shown that the coloration of 2,3,5-triphenyltetrazolium chloride is independent of the dose rate, increasing the dose via the beam current.

3 Methods

3.1 Flow cytometry and analysis

Flow cytometry is a technique used in cell biology laboratories to count and characterize cells or other microbiological organisms. It can be used to count and analyze single particles with diameters of a few micrometers. Liquid samples containing cells or particles pass through a fluidic system where the particles are aligned and passed through a laser beam, with one particle at a time. The laser light scattered by each particle is detected. By measuring the intensity and direction of the light, the size and internal complexity of the cell or particle can be determined. Flow cytometers measure forward scatter (FSC)—a relative unit of size—and sideward scatter (SSC), a relative unit of granularity. Using flow cytometry software, the scatter of multiple cells or particles can be visualized in scatter dot plots with FSC and SSC values on the axis. Particles of similar size and shape appear as clouds in the scatter dot plots and can be distinguished from other possible particles in the samples or contaminants. In addition, the scattered fluorescence intensity of each particle can be measured either in the hole sample or for particles with specific scattering characteristics. Before measuring fluorescence intensities, the cloud in the scatter dot plots can be selected, called gating. This ensures that only the fluorescence intensities of a region of interest are included in the analysis. Fluorescence intensities can be measured in different channels at specific emission wavelengths [21].

In this study, single-particle analysis was performed on the BD Accuri C6 Plus Flow Cytometer (Becton, Dickinson and Company, California, United States) using BD Accuri C6 Plus software. First, scatter dot plots were recorded to identify the 6-μm-diameter beads and gated. The percentage of particles within the gates was recorded. The fluorescence intensities of the beads from the gates were detected in the so-called FITC channel, named after a green fluorochrome, with a fixed emission wavelength of 533 nm. The measurements of each sample took approximately 10 min.

After high-energy electron irradiation, we established a calibration curve from the mean fluorescence values at 533 nm (FITC-A), measured within the gates of the scatter dot plots. We marked the regions of interest of 0 kGy, 10 kGy, 30 kGy, and 50 kGy in the histograms.

3.2 Irradiation

3.2.1 High-energy electron irradiation

Batches of 230 μL were pipetted into the Petri dish setup and irradiated at 10 kGy, 30 kGy, and 50 kGy. A reference sample was also analyzed and transferred in this setup, but it was not irradiated (0 kGy). The dose was varied by the beam current, which determines the dose rate under the beam, the transport velocity for a defined passage of the samples under the beam, which affects the duration of a single irradiation cycle, and the total number of runs (see

parameters given in Table 3). The dose rates $\dot{D}$ were estimated from the given dose D per run under the electron beam, length y, and transport velocity v. The length y was estimated from the normalized distribution of the beam intensity in [22]. Therefore, a region of 95.4% dose was chosen. This estimation yielded dose rates of $0.55 \cdot 10^3$ Gy/s for 10 kGy and $1.09 \cdot 10^3$ Gy/s for 30 kGy and 50 kGy.

$$\dot{D} = D \cdot \frac{v}{y}. \tag{1}$$

3.2.2 Cumulative irradiation at low energy to test the dose linearity of fluorescence intensities

In order to test dose dependency, the samples were irradiated in the REAMODE with constant parameters (Table 3) but different numbers of runs. This method was used to accumulate the dose. Two samples were irradiated for each dose, and each sample was measured three times so that the average signal was calculated from six values. The reference film dosimeter was irradiated simultaneously. The mean dose rate per sample was estimated to be $1.73 \cdot 10^3$ Gy/s. This was calculated using Equation 1.

3.2.3 Low-energy electron irradiation in a microfluidic chip

For each dose, 5 mL of the bead suspension was transported through the microfluidic chip. To increase the dose, the beam current was increased, while all other parameters were kept constant (see parameters given in Table 3). The beam current was varied from 0.30 mA to 1.25 mA, yielding mean dose values from 5 kGy to 30 kGy.

The dose rates were estimated to range from $0.28 \cdot 10^3$ Gy/s to $12.2 \cdot 10^3$ Gy/s, as given in Equation 2. Here, D refers to the dose measured by the liquid dosimeter, σ determines the cross section of the channels in the microfluidic channel perpendicular to the flow, l is the length of the channels under the electron exit window, and Φ is the volume flow, which was calculated from the overall sample volume V_{sample} of 5 mL and the time of process t of 21 s.

$$\dot{D} = D \cdot \frac{\Phi}{\sigma \cdot l} \quad with \quad \Phi = \frac{V_{sample}}{t}. \tag{2}$$

The experiment was performed in duplicate. The same irradiation setup and procedure were used for the irradiation of the alternative polymer beads (microParticles GmbH and PolyAn GmbH, Berlin, Germany).

3.3 Evaluation of dose distribution

The response curve fit obtained from high-energy electron irradiation was used to calculate the fluorescence intensities ($FITC - A_{calc}$) for smaller dose intervals: 5 kGy, 10 kGy, 20 kGy, 30 kGy, 40 kGy, and 50 kGy.

The lower borders ($FITC - A_{lower\ border}$) and upper borders ($FITC - A_{upper\ border}$) for the fluorescence intensities of each dose interval were calculated by subtracting (lower borders) and adding (upper borders) the product of mean of the coefficients of variation (CV_{mean}) of the fluorescence intensities and $FITC - A_{calc}$ (Equation 3).

$$FITC - A_{lower\ border} = FITC - A_{calc} - (CV_{mean} \cdot FITC - A_{calc});$$
$$FITC - A_{upper\ border} = FITC - A_{calc} + (CV_{mean} \cdot FITC - A_{calc}). \tag{3}$$

TABLE 3 Parameters and dose values of high-energy electron irradiation at the Leibniz Institute of Polymer Research Dresden, the low-energy electron irradiation in the microfluidic chip of the ELLI300 instrument in Leipzig, and low-energy electron irradiation REAMODE instrument at Fraunhofer FEP in Dresden.

High-energy electron irradiation at ELV-2			
1.5 MeV acceleration voltage			
75 Hz scan frequency			
20-cm distance to the titanium exit window			
I [mA]	Transport velocity v [mm/s]	Number of runs	D [kGy]
2.0	55	2	10
4.0	36	2	30
4.0	44	4	50
Low-energy electron irradiation at ELLI300 in the microfluidic chip			
300 kV acceleration voltage			
57 mm/s conveyor speed			
45-mm distance to the electron exit window (air gap)			
I [mA]		D [kGy]	
0.00		0.0	
0.30		5.3	
0.50		12	
0.75		18	
0.90		22	
1.00		25	
1.25		30	
Low-energy electron irradiation at REAMODE			
200 keV acceleration voltage			
155 mm/s conveyor speed			
45-cm distance to the titanium exit window			
I [mA]	Number of runs		D [kGy]
1.5	2		10
1.5	4		20
1.5	6		30

TABLE 4 Beam current I, minimum, maximum, and mean dose values estimated from the fluorescence measurements of the beads, reference dose D_{Ref} estimated from the radiochromic liquid dosimeter based on 2,3,5-triphenyltetrazolium chloride.

I [mA]	D_{min} [kGy]	D_{max} [kGy]	D_{mean} [kGy]	D_{Ref} [kGy]
0.00	0.89	2.5	1.7	0
0.00	0.69	2.4	1.5	0
0.30	1.8	6.7	4.2	5.3
0.30	2.0	5.8	3.9	
0.50	1.9	12	7.0	12
0.50	6.5	18	12	
0.75	6.4	19	13	18
0.75	6.5	18	12	
0.90	10	24	17	22
0.90	7.5	27	17	
1.00	11	28	19	25
1.00	11	30	20	
1.25	14	29	22	30
1.25	12	33	23	

in bar diagrams with the amounts of particles in the y-axis and the allocation to the theoretical dose peak in the x-axis. This was performed for the different irradiated samples referring to the mean reference dose values.

To determine minimum and maximum fluorescence intensities (FITC-A), the standard deviation (SSD) was subtracted or added from the mean fluorescence intensity ($FITC-A_{Mean}$). The SSD was calculated from the coefficient of variation (CV) and mean fluorescence intensity (Equation 4), which were calculated using flow cytometry software from the single events. Finally, the minimum and maximum doses were derived from the response function. The doses were determined as 185, as shown in Table 4.

$$SSD = CV \cdot FITC - A_{Mean}.   (4)$$

3.4 Accuracy of the liquid reference dosimeter

Before 2,3,5-triphenyltetrazolium chloride was used as a liquid reference dosimeter in the microfluidic chip, its dose rate dependence was tested at the low-energy electron irradiator REAMODE at Fraunhofer FEP. In two experiments, the dosimeter was irradiated with two constant beam currents of 3 mA and 0.6 mA, while the dose was varied via the conveyor speed. Those parameters yielded estimated constant mean dose rates of 3,870 Gy/s and

Those new regions of interest were saved in the flow cytometric software program. The fluorescence intensities in the FITC-A channel after LEEI in the microfluidic chip were counted and allocated to the regions of interest. The results were visualized

713 Gy/s. In two further experiments, the liquid dosimeter samples were irradiated at a constant conveyor speed, but the dose was varied by increasing the beam current and dose rate (approximately from 392 Gy/s to 4,068 Gy/s). The change in absorbance was calculated by subtracting the absorbance before irradiation from the absorbance after exposure.

3.5 Statistics and uncertainty budget

From the FITC channel, the fluorescence spectra were generated, and the mean fluorescence intensity ($FITC - A_{Mean}$) and its CV were calculated during counting using the software program from the measurements of the single-fluorescence intensities ($FITC - A_i$) of each particles flowing through the laser (Equation 5).

$$CV = \frac{SSD}{FITC - A_{Mean}} \cdot 100\% \ with \ SSD = \sqrt{\sum_{k=1}^{i} \left(FITC - A_i - FITC - A_{Mean} \right)^2}. \tag{5}$$

Then, the areas in the spectra could be assigned to dose values. We established an uncertainty budget according to the CIRM 29 guidelines for calibration [23]. Components of uncertainties of the calibration of the bead-based dosimeter by irradiation at high energies were identified and assigned to the uncertainties of types A and B.

3.5.1 Uncertainty of the irradiation facility

The combined uncertainty (u_c) of the irradiation facility was calculated from the sum of the components of uncertainty (u_i) of the beam current, beam voltage, conveyor speed, beam field uniformity, and dose gradient using Equation 6.

$$u_c = \sqrt{\sum (u_i)^2}. \tag{6}$$

3.5.2 Uncertainty of the liquid bead dosimeter

The uncertainty of the bead-based dosimeter was calculated as a combined uncertainty (Equation 6) of the uncertainty of the thickness of the liquid film and the variation in the initial fluorescence intensity. The uncertainty of the thickness of the liquid film was estimated as the type B uncertainty, given by the pipetting uncertainty of the systematic and random error of the Eppendorf pipettes given in the manual. The standard uncertainty of type B ($u_{std}(Type \ \ B)$) is calculated by Equation 7 [23].

$$u_{std}(Type \ \ B) = \frac{u_i}{\sqrt{3}}. \tag{7}$$

The uncertainty of the initial fluorescence intensity was calculated as a sum of squares from the CVs of the mean fluorescence intensities at 0 kGy, 10 kGy, 30 kGy, and 50 kGy.

3.5.3 Uncertainty of flow cytometry

The uncertainty of flow cytometry was estimated from the maximal fluorescence precision of the cytometer, which was provided by the manufacturer.

3.5.4 Uncertainty of the calibration curve

The uncertainty of calibration fitting was estimated from the dosimeter-to-dosimeter scatter (Equation 8). Therefore, the uncertainty was calculated from the sum of squares of the residuals, calculated as in Equation 9, divided by the number of dosimeters n_d and subtracted by the number of coefficients of the fit n_c. The latter had a value of 1 as it was a linear fit.

$$u = \sqrt{\frac{\sum residuals^2}{n_d - n_c}}, \tag{8}$$

$$residuals\,[\%] = \frac{D_{calculated} - D_{delivered}}{D_{delivered}} \cdot 100. \tag{9}$$

4 Results
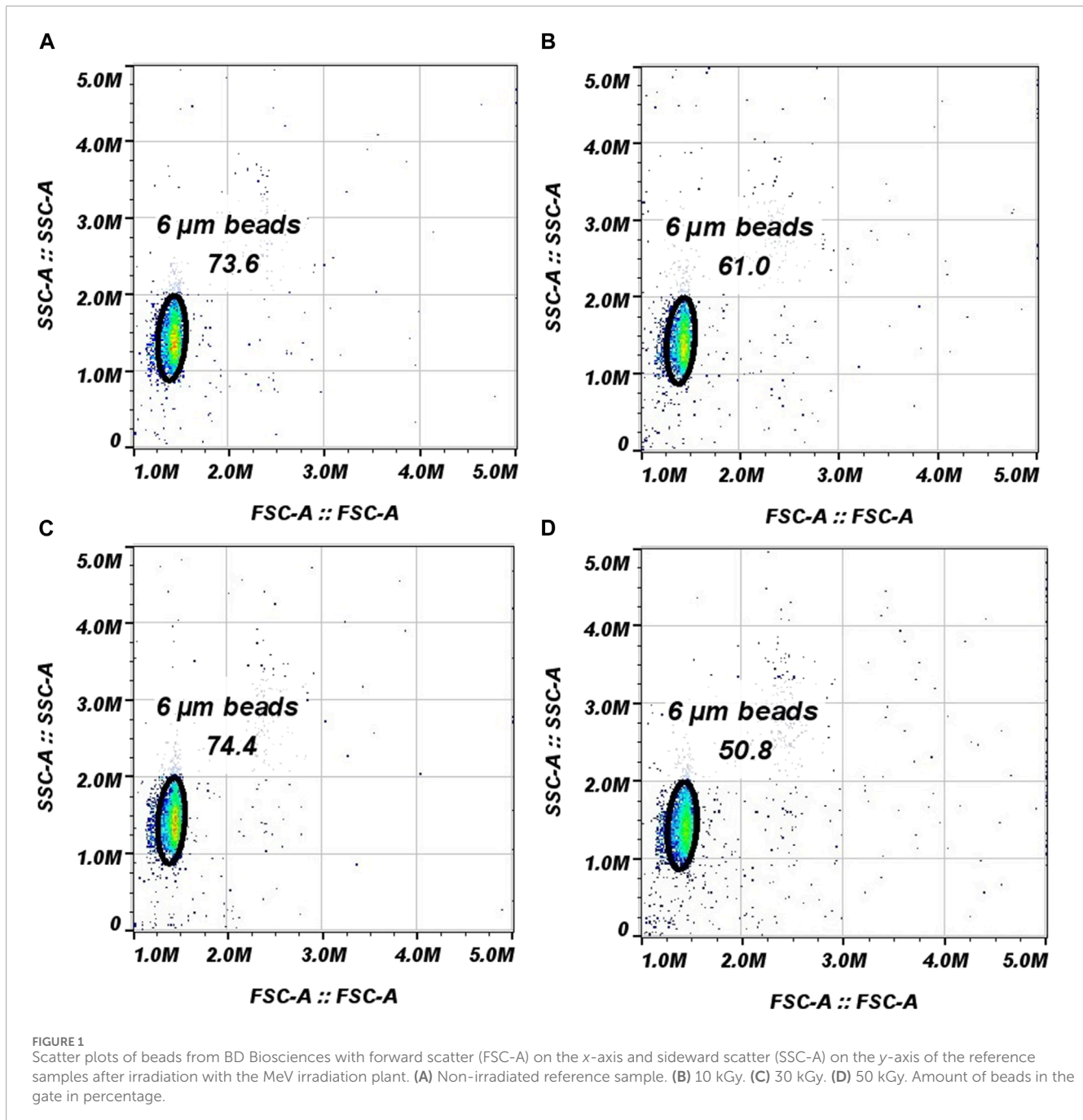
4.1 Gating of the beads

The main clouds above 1,000.000 FSC and approximately 2,000.000 SSC appeared in the scatter plots (Figure 1). Beads that were detected in a specific area marked with black circles were gated. In the dot plots of the unirradiated reference samples, approximately 74% (Figure 1A) of all events counted was assigned to that gate. The gate remained valid after irradiation with 10 kGy (Figure 1B) and 30 kGy (Figure 1C) as the main cloud appeared in this area. This indicated that the shape and size of the beads were not altered by irradiation. However, the number of beads detected in the gate decreased after exposure to a dose of 50 kGy, where less than 51% beads were detected in the gate (Figure 1D).

4.2 Impact of irradiation on fluorescence

The irradiation of the beads with defined dose values by the high-energy irradiation plant caused an impact on the fluorescence intensities. The histogram of the non-irradiated reference sample, which only recognized the counts of the previously defined gate (E1), showed a defined peak at the mean fluorescence intensity (at 533/30 nm) of 616 FTIC-A (Table 5), which is highlighted in green in Figure 2. A total of 98.8% of the counts detected in the gate was located in this green peak. An amount of 0.5% of the counts showed a higher fluorescence signal, while the remaining count may have weaker fluorescence. This indicates the presence of noise particles.

When comparing the samples irradiated with three different dose values (10 kGy, 30 kGy, and 50 kGy), we observed a shift toward areas of higher fluorescence intensity (Figure 2). The mean fluorescence increased with the dose. After exposure to 10 kGy (red peak), the mean fluorescence was twice as high as the mean signals of the reference sample; after 30 kGy (blue peak) and 50 kGy (yellow peak), it further increased (see also Table 5). The coefficient of variation, which was obtained using BD Accuri C6 Plus Analysis software, determines the width of the peaks. The coefficient of variation was used to calculate the standard deviations (Table 5).

The mean fluorescence intensities at 533 nm within the gating for each dose (Table 5) were fitted with a linear function from

FIGURE 1
Scatter plots of beads from BD Biosciences with forward scatter (FSC-A) on the *x*-axis and sideward scatter (SSC-A) on the *y*-axis of the reference samples after irradiation with the MeV irradiation plant. **(A)** Non-irradiated reference sample. **(B)** 10 kGy. **(C)** 30 kGy. **(D)** 50 kGy. Amount of beads in the gate in percentage.

0 to 50 kGy. The single-fluorescence intensities (n = 1,000) are plotted in Figure 3. A dose calibration function was derived from the linear function of the mean FITC-A (the dose response) and the reference dose measured using the Crosslinking dosimeter.

4.3 Dose linearity of fluorescence intensities by cumulative irradiation

The fluorescence intensities of the beads increased linearly with the dose applied (Figure 4), although the dose rate was constant. This indicated that the dose, rather than the dose rate, induced the response of the dosimeter.

4.4 Evaluation using low-energy electron irradiation in a microfluidic chip

The fluorescence intensities (FITC-A) increased linearly over a dose range between 0 and 30 kGy (Figure 5). However, the fluorescence intensity values were widespread, and those at the higher dose levels overlap with those at lower doses.

In order to perform dose mapping within the microfluidic chip, the fluorescence intensities were mapped to dose regions of interest of 0 kGy, 5 kGy, 10 kGy, 20 kGy, 30 kGy, 40 kGy, and 50 kGy (Table 6).

After radiation exposure of 5 kGy (mean dose measured by 2,3,5-triphenyltetrazolium chloride), proportions of 25% of the

TABLE 5 Dose and mean fluorescence (FITC-A) with the standard deviation (SD) and coefficient of variation (CV).

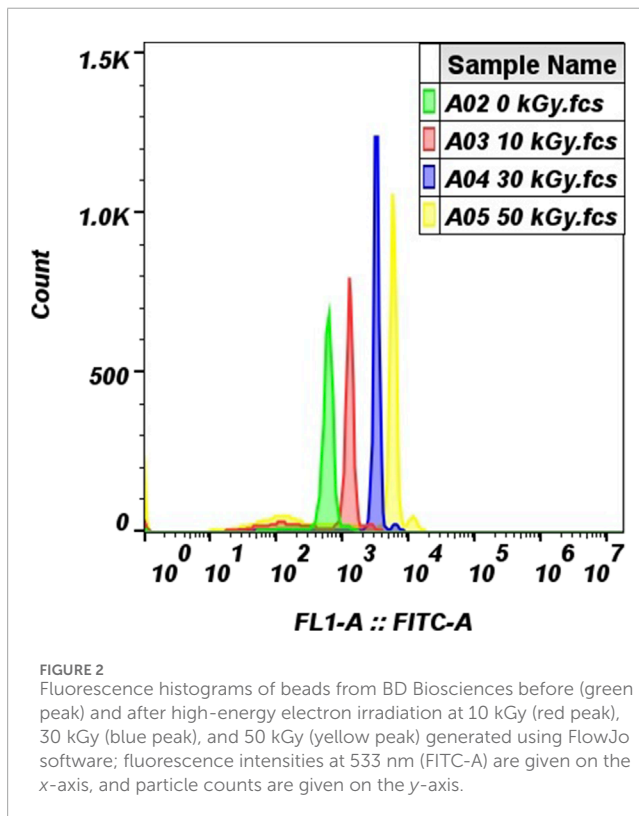| Dose	Mean FITC-A	SD FITC-A	CV FITC-A [%]
0 kGy	616	89.14	14.47
10 kGy	1,286	148.9	11.58
30 kGy	3,260	347.8	10.67
50 kGy	5,848	1,109	18.96

FIGURE 2
Fluorescence histograms of beads from BD Biosciences before (green peak) and after high-energy electron irradiation at 10 kGy (red peak), 30 kGy (blue peak), and 50 kGy (yellow peak) generated using FlowJo software; fluorescence intensities at 533 nm (FITC-A) are given on the x-axis, and particle counts are given on the y-axis.

FIGURE 3
Linearity between single-fluorescence intensities (n = 1,000), measured at 533 nm (FITC-A), on the y-axis and the reference dose in kGy on the x-axis.

FIGURE 4
Cumulative irradiation of beads from BD Biosciences. Fluorescence (mean FITC-A) on the y-axis and mean reference dose on the x-axis after low-energy electron irradiation at REAMODE.

beads had fluorescence values correlating with 5 kGy, while large quantities did not receive a dose, and a minor amount received 10 kGy (Table 6). Although the dose obtained from the reference dosimeter was 12 kGy, the dose was mainly distributed within the 5-kGy area, with approximately 45% and 20% assigned to 10 kGy (Table 6). A majority of the beads (40%) were allocated to the 20-kGy region of interest if a dose of 22 kGy was applied (Table 6). After irradiation with a mean reference dose of 30 kGy, the dose distribution was mainly located at 20 kGy, and about 20% received a dose of approximately 30 kGy. Particles were found in the 50-kGy allocation as well (Table 6). The dose distribution of the second run was slightly different from that of the first run (compare upper rows of Table 6 and lower rows of Table 6). The deviation of the fluorescence intensities was 10% at doses up to 30 kGy and 18% for a dose of 50 kGy. This also indicates that the beads in the upper liquid layers receive higher doses, and those in the lower layers receive lower doses due to the steep dose gradient. The dose gradient of the
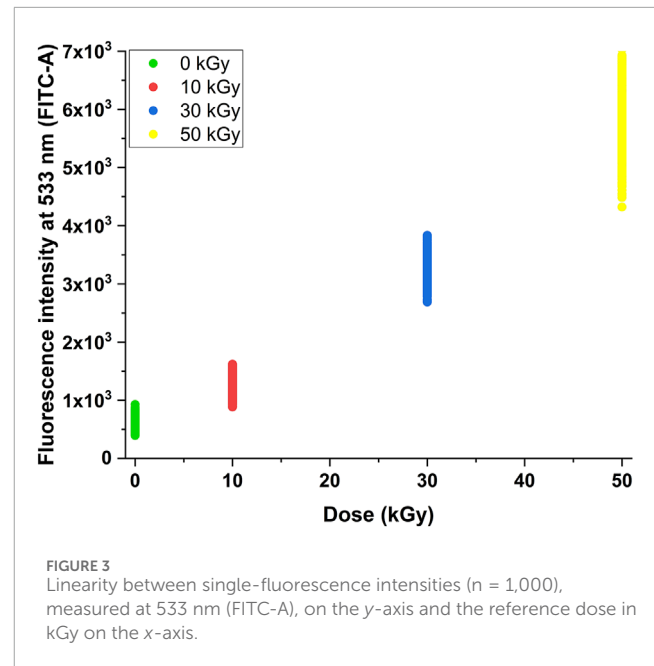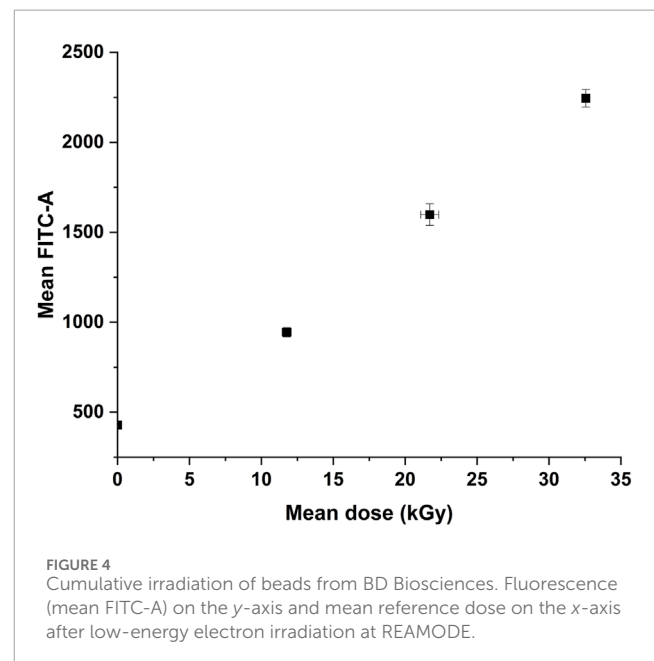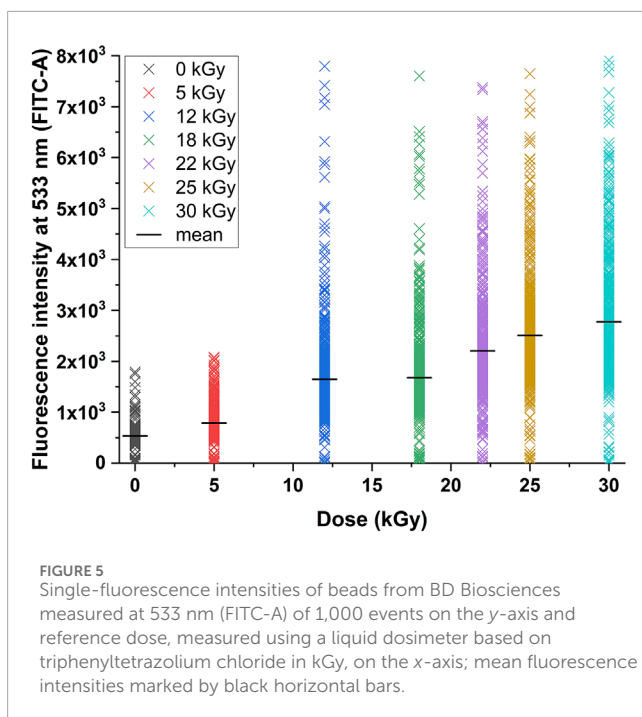
low-energy electrons within the 200-µm microfluidic channels was estimated to be 5% (Supplementary Material S1).

4.5 Impact of irradiation on fluorescence on alternative polymer beads

Other than the beads from BD, the fluorescence intensities of polymethyl methacrylate beads purchased from two other companies (microParticles GmbH and PolyAn) did not increase (Figure 6). For those beads, no impact of the irradiation on fluorescence was found.

FIGURE 5
Single-fluorescence intensities of beads from BD Biosciences measured at 533 nm (FITC-A) of 1,000 events on the *y*-axis and reference dose, measured using a liquid dosimeter based on triphenyltetrazolium chloride in kGy, on the *x*-axis; mean fluorescence intensities marked by black horizontal bars.

4.6 Accuracy of the liquid reference dosimeter

The change in the absorbance of the liquid dosimeter 2,3,5-triphenyltetrazolium chloride increased linearly in a dose range of 5 kGy–30 kGy of low-energy electron irradiation in the REAMODE. The dosimeter was best suited for this range, and we chose it as the reference dosimeter for the subsequent irradiation in the microfluidic chip at low energy. The linear dose dependence is the same for all investigated currents and, thus, independent of the dose rate. Accordingly, dose rate effects play a minor role up to 30 kGy.

4.7 Uncertainty budget of the calibration at high energy

The uncertainty budget (Table 7) of the experiments at the MeV electron beam instrument was established from components of each step: the calibration of the reference dosimeter, irradiation facility, liquid bead dosimeter, measurements obtained by flow cytometry, and calibration of the bead-based dosimeter.

4.7.1 Calibration of the reference dosimeter
The uncertainty of the reference film dosimeters was taken as 5%.

4.7.2 Irradiation facility
Uncertainties regarding the irradiation facility included the dose gradient and the acceleration voltage of the electron accelerator. Another component of uncertainties was the dose gradient, which could be estimated from the uncertainty due to the beam current. Other components were the beam inhomogeneity, dose gradient, and conveyor speed. The combined uncertainty of these

components was estimated to be 3.3%. However, the temperature during irradiation was a type-B uncertainty component, but it was neglected.

4.7.3 Uncertainty of the liquid bead dosimeter
The uncertainty of the liquid bead dosimeter was calculated from the liquid film thickness and the variation in the fluorescence signal (FITC-A) measured by the flow cytometer. The component of film thickness was due to pipetting and was 0.45% ($k = \sqrt{3}$; rectangular distribution). The standard uncertainty of the fluorescence signal was assumed to be 29% in total. This was calculated from the sum of squares of each CV of the FITC-A value provided by flow cytometer software (uncertainty of type A).

4.7.4 Flow cytometry
The measurement of the beads by flow cytometry was also a contributor to the uncertainty budget. Here, the maximum precision of the fluorescence measurement was reported as 3.0%, which corresponds to an uncertainty of type B. Other uncertainties might include the Gaussian intensity profile of laser excitation, which might lead to different rates of excitation of the beads, or Rayleigh and Raman scattering of the solvent [24, 25]. However, these uncertainties were neglected in the uncertainty budget.

4.7.5 Uncertainty of the calibration curve
Finally, the uncertainty of the calibration curve was estimated to be 12.2% ($k = 1$) from the curve fitting. The combined standard uncertainty ($k = 1$) was 31% in total (Table 7).
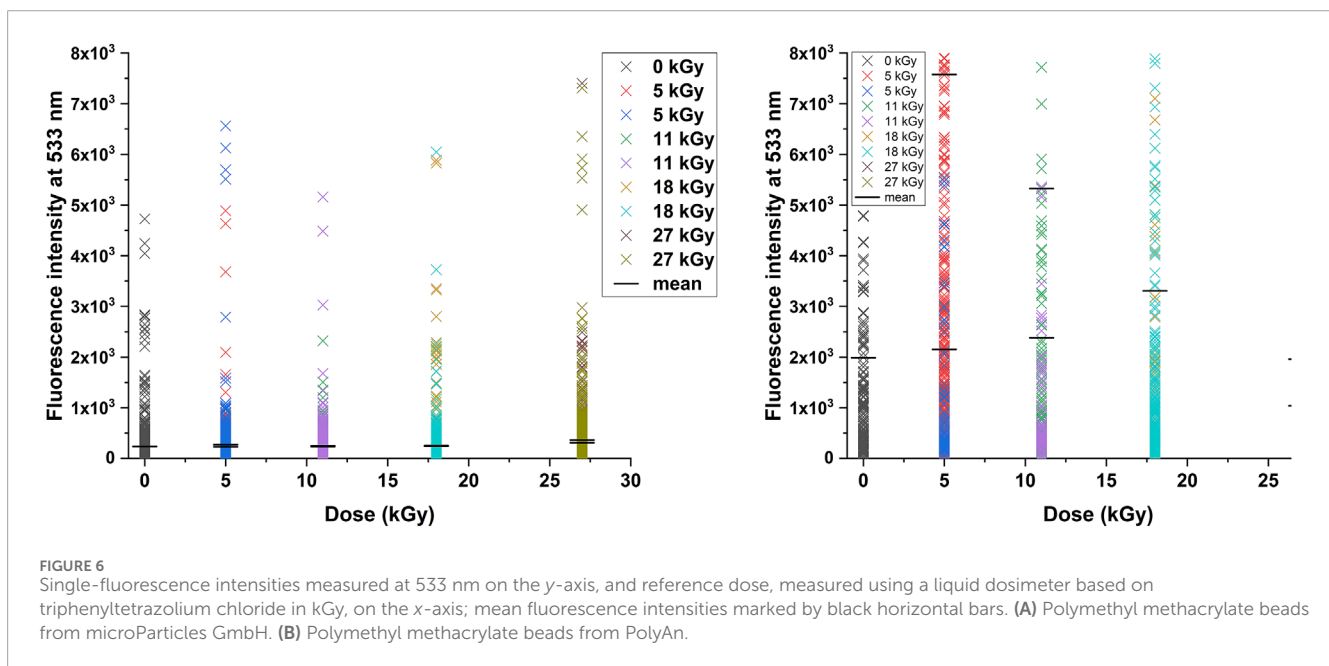
5 Discussion

In this study, we demonstrated the applicability of our method to determine the relative dose distribution in a dynamic irradiation instrument by diluted polymer beads and flow cytometric measurements. A linear calibration function was found by high-energy irradiation in a static setup of Petri dishes in the dose range of 10–50 kGy. The calibration function was used to estimate the mean doses and minimum and maximum dose values in a dynamic microfluidic module for LEEI. Furthermore, it was possible to assign the amounts of beads to specific dose levels up to 50 kGy. The beads were also tested at a constant dose rate in the REAMODE, and a linear response to the absorbed dose was demonstrated. Beads of other suppliers made of polymethyl methacrylate with similar size were tested but did not show the same functionality.

The dot plots of the reference samples and the samples, which were irradiated using the high-energy electron beam, showed particles outside the gates. These could be small impurities. The amount of those detected outside the gate seemed to increase with high dose, which could be an indication of damage to the beads due to the radiation. This was observed in the samples of after irradiation in the two LEEI facilities as well. There is the risk that the beads agglomerate. Agglomerated beads or worse distribution may affect the deep dose distribution and penetration depths of the electrons. However, this effect can be neglected because previous light microscopy studies (two drops of bead suspension in 2 mL of FACS flow solution) showed low agglomeration before irradiation in any setup. It was assumed that agglomeration is even less likely

TABLE 6 Dose distribution of beads from BD Biosciences irradiated with the low-energy electron beam in a microfluidic chip: 0 kGy, 5 kGy, 12 kGy, 22 kGy, and 30 kGy. Relative count of beads allocated to the dose peaks (0 kGy, 5 kGy, 10 kGy, 20 kGy, 30 kGy, 40 kGy, and 50 kGy) in percentage. The dose was varied via the beam current.

D_{ref}	Particle count at the dose peak [%]						
	0 kGy	5 kGy	10 kGy	20 kGy	30 kGy	40 kGy	50 kGy
First run							
0 kGy	52.00	0.00	0.00	0.00	0.00	0.00	0.00
5 kGy	32.00	26.00	4.00	0.00	0.00	0.00	0.00
12 kGy	4.17	43.75	22.92	2.08	0.00	2.08	0.00
22 kGy	2.00	2.00	12.00	40.00	14.00	4.00	0.00
30 kGy	0.00	0.00	2.00	40.00	20.00	10.00	2.00
Second run							
0 kGy	50.10	0.00	0.00	0.00	0.00	0.00	0.00
5 kGy	29.52	28.72	6.23	0.20	0.00	0.00	0.00
12 kGy	0.60	4.42	39.96	15.46	3.61	0.60	0.00
22 kGy	1.41	2.21	7.83	41.17	10.04	4.02	1.00
30 kGy	0.00	0.60	2.19	33.47	21.12	11.55	4.38

FIGURE 6
Single-fluorescence intensities measured at 533 nm on the *y*-axis, and reference dose, measured using a liquid dosimeter based on triphenyltetrazolium chloride in kGy, on the *x*-axis; mean fluorescence intensities marked by black horizontal bars. **(A)** Polymethyl methacrylate beads from microParticles GmbH. **(B)** Polymethyl methacrylate beads from PolyAn.

with higher dilution, which was used in the microfluidic chip. In addition, agglomerated beads were not considered in the analysis by flow cytometry. The flow cytometer filters odd particles that are not spherical, and the gating in the scatter dot plots ensured the fluorescence measurements at defined sizes. Regarding the tests of the calibrated beads in the microfluidic chip at low energy, it should be noted that the dose rate and stopping power were different.

While the stopping power in water with polymethyl methacrylate (< 1%) of the 300-keV electron beam was 2.36 MeV cm^2/g, it was 1.84 MeV cm^2/g for the 1.5-MeV electron beam. The stopping power of the low-energy irradiation was approximately 28% higher (Supplementary Material S2). Furthermore, the dose gradient of low-energy irradiation was steeper. This effect was minimized by the chip design with channels less than 200-μm thick. Water was

TABLE 7 Uncertainty budget of the calibration of the bead-based dosimeter with standard uncertainties, divisors k, sensitivity factors c, combined uncertainties, and expanded uncertainties.

Component	Value [%]	k	c	Uncertainty [%]	Type
Calibration reference dosimeter	5.0	2	1	2.5	B
Irradiation facility					
Beam current	2.5	$\sqrt{3}$	1	1.4	B
Beam voltage	0.53	$\sqrt{3}$	1	0.31	B
Conveyor speed	0.60	$\sqrt{3}$	1	0.35	B
Beam homogeneity	5.0	$\sqrt{3}$	1	2.9	B
Dose gradient (within liquid)	0.02	$\sqrt{3}$	1	0.01	B
Combined				3.3	
Bead dosimeter					
Thickness of the liquid film	0.78	$\sqrt{3}$	1	0.45	B
CV fluorescence intensity	29	1	1	29	A
Combined				29	
Flow cytometry					
Precision of fluorescence	3.0	$\sqrt{3}$	1	1.7	B
Calibration					
Curve fitting	12	1	1	12	A
Total [%]	**31**				
Expanded (k = 2) [%]	**63**				

assumed to have its maximum dose within the fluidic channels, and a dose gradient of 2.28% was estimated (compare the theoretical dose depth in Supplementary Material S1). However, it may be possible that some energy reaches the liquid dosimeters before reaching the channels, which would result in the overestimation of the dose rates. Another difference between the irradiation with the low-energy electron beam in the microfluidic chip and the high-energy electron irradiation in Petri dishes is the required dilution of the bead suspension to obtain larger volumes. Although up to 9,500 beads per sample were measured after high-energy irradiation, the number of beads measured per sample was set to 50 after LEEI using ELLI300. Uncertainties in irradiation at low energy can affect the results. These include the accuracy of the liquid reference dosimeter, which is not as accurate as high-standard dosimeters, and the beam homogeneity. The dose distributions between 10 kGy and 30 kGy, 30 kGy and 50 kGy, and above have not been investigated yet. The number of beads detected in the scattering plots decreased after exposure to a dose of 50 kGy. This could be explained as some beads might degrade due to the high dose. For a more detailed statistical analysis and reduction in uncertainties, the sample size and the number of replicates could be increased. It should be mentioned that other beads made of polymethyl methacrylate have not worked as dosimeters, and it is known from the literature that polymethyl methacrylate has a relatively weak autofluorescence [26], and the autofluorescence depends on the fabrication process [27]. The exact working mechanism of the bead-based dosimeter has not yet been determined.

The uncertainty budget in this study determined an overall uncertainty of the mean dose values of 31% (k = 1), which was mainly due to the coefficient of variation of the fluorescence intensities with 29%. Another major component was the fit of the calibration function of 12%. However, this could be further improved by recognizing more dose points, as recommended by [23]. In the literature, uncertainties of commercial luminescence dosimeters were described with 5%, for example, glass beads with radiophotoluminescent or thermoluminescent signals [16, 28]. Other dosimeters, such as thermoluminescent materials, for instance, lithium fluoride, have uncertainties of 10% [29]. For some applications and luminescent dosimeters, the reproducibility could even be below 1%, but the precision and accuracy rely on a range of different factors, including the reading process [12]. Furthermore, the size and shape of the dosimeter have an impact on its

performance. Nevertheless, the radiation response was not saturated at 30 kGy as it is the case for common thermoluminescent phosphors [30] and radio photoluminescent glass beads, for instance [16]. On the whole, with this study, a proof-of-concept of a novel flowing-type liquid dosimetry system, which was the determination of dose distribution of low-energy electron irradiation of liquids at high dose, was shown.

6 Conclusion

In conclusion, the liquid dosimeter based on suspended beads made of polymethyl methacrylate showed an increase in fluorescence intensity within 10 kGy–50 kGy. The linear dose response was found after irradiation by high-energy electron irradiation. The dosimeter system using flow cytometry, which provides dose measurements of each single bead, was tested in a microfluidic setup using low-energy electron irradiation. A dose distribution including minimal, maximal, and mean dose values was found. This new technique for determining dose distribution in liquids is based on measuring the radiation response of each particle in a sample and calculating the dose individually. The dose and dose rate dependence of the beads were tested as well, and a minor dependence on the dose rate was found. Advantages for using polymers can be formed in very small beads in the micrometer scale, so they can be used for microfluidic applications, and they are suitable for low-energy electron irradiation due to low-density polymer beads. In addition, polymer beads were distributed well in the liquids and less likely to sediment like more dense materials, such as glasses or ceramics, which is an advantage for their handling and processing. The use of flow cytometry allowed fast measurements and gating of the beads from their scattering properties, which would allow measurements of samples containing other populations. Although uncertainty could be further improved, the bead-based dosimeter showed the best performance for quality control within the 10 kGy–30-kGy mean dose for biotechnological or pharmaceutical applications.

In further improvements, it is desirable to recognize the geometrical location of such beads to perform spatially resolved dose mapping, which was not possible with the proposed analysis yet.

Data availability statement

The original contributions presented in the study are included in the article/Supplementary Material; further inquiries can be directed to the corresponding author.

Author contributions

JB: data curation, investigation, visualization, writing–original draft, writing–review and editing, and methodology. LK: data curation, investigation, methodology, and writing–review and editing. AP: investigation and writing–review and editing. JS: investigation and writing–review and editing. TT: data curation and writing–review and editing. MT: methodology and writing–review and editing. TG: methodology and writing–review and editing. EH: supervision and writing–review and editing. UK: conceptualization and writing–review and editing. BP: supervision and writing–review and editing. SS: conceptualization, supervision, and writing–review and editing.

Funding

Acknowledgments

Conflict of interest

The authors declare that the research was conducted in the absence of any commercial or financial relationships that could be construed as a potential conflict of interest.

The author(s) declared that they were an editorial board member of Frontiers, at the time of submission. This had no impact on the peer review process and the final decision.

Publisher's note

Supplementary Material

The Supplementary Material for this article can be found online at: https://www.frontiersin.org/articles/10.3389/fphy.2024.1490048/full#supplementary-material.

References

1. Schiller S, Heisig U, Panzer S. *Electron beam technology. A Wiley-Interscience publication*. New York: Wiley (1982).

2. Fertey J, Bayer L, Grunwald T, Pohl A, Beckmann J, Gotzmann G, et al. Pathogens inactivated by low-energy-electron irradiation maintain antigenic properties and induce protective immune responses. *Viruses* (2016) 8:319. doi:10.3390/v8110319

3. Fertey J, Thoma M, Beckmann J, Bayer L, Finkensieper J, Reißhauer S, et al. Automated application of low energy electron irradiation enables inactivation of pathogen- and cell-containing liquids in biomedical research and production facilities. *Scientific Rep* (2020) 10:12786. doi:10.1038/s41598-020-69347-7

4. Eberlein V, Ahrends M, Bayer L, Finkensieper J, Besecke J, Mansuroglu Y, et al. Mucosal application of a low-energy electron inactivated respiratory syncytial virus vaccine shows protective efficacy in an animal model. *Viruses* (2023) 15:1846–17. doi:10.3390/v15091846

5. Walcher L, Kistenmacher A, Sommer C, Böhlen S, Ziemann C, Dehmel S, et al. Low energy electron irradiation is a potent alternative to gamma irradiation for the inactivation of (car-)nk-92 cells in atmp manufacturing. *Front Immunol* (2021) 12:684052. doi:10.3389/fimmu.2021.684052

6. Schopf S, Gotzmann G, Dietze M, Gerschke S, Kenner L, König U. Investigations into the suitability of bacterial suspensions as biological indicators for low-energy electron irradiation. *Front Immunol* (2022) 13:814767. doi:10.3389/fimmu.2022.814767

7. Laurell B, Föll E, editors. *Dosimeter overview and the use of dμ for calibration*. Electron Crosslinking AB (2009).

8. McLaughlin WL, editor. *Radiation processing dosimetry - past, present and future*. IAEA-TECDOC (1999).

9. Precek M, Kubelik P, Vysin L, Schmidhammer U, Larbre JP, Demarque A, et al. Dose rate effects in fluorescence chemical dosimeters exposed to picosecond electron pulses: an accurate measurement of low doses at high dose rates. *Radiat Res Soc* (2022) 197:131–48. doi:10.1667/RADE-20-00292.1

10. Krieger H. *Strahlungsmessung und Dosimetrie: Studium*. Wiesbaden: Vieweg + Teubner (2011). 1. aufl. edn.

11. Yanagida T, Okada G, Kato T, Nakauchi D, Kawaguchi N. A review and future of rpl dosimetry. *Radiat Measurements* (2022) 158:106847. doi:10.1016/j.radmeas.2022.106847

12. Yukihara EG, McKeever SWS, Andersen CE, Bos AJJ, Bailiff IK, Yoshimura EM, et al. Luminescence dosimetry. *Nat Rev Methods Primers* (2022) 2:26. doi:10.1038/s43586-022-00102-0

13. Huang DY, Hsu SM. *Radio-photoluminescence glass dosimeter (RPLGD)*. IntechOpen (2011) doi:10.5772/23710

14. Liu H, Qin H, Shen N, Yan S, Wang Y, Yin X, et al. Emergence of a radical–stabilizing metal–organic framework as a radio–photoluminescence dosimeter. *Angew Chem Int Edition* (2020) 59:15209–14. doi:10.1002/anie.202006380

15. Iwao M, Takase H, Shiratori D, Nakauchi D, Kato T, Kawaguchi N, et al. Ag-doped phosphate glass with high weathering resistance for rpl dosimeter. *Radiat Measurements* (2021) 140:106492. doi:10.1016/j.radmeas.2020.106492

16. Pramberger D, Aguiar YQ, Trummer J, Vincke H. Characterization of radio-photo-luminescence (rpl) dosimeters as radiation monitors in the cern accelerator complex. *IEEE Trans Nucl Sci* (2022) 69:1618–24. doi:10.1109/tns.2022.3174784

17. Jafari SM, Bradley DA, Gouldstone CA, Sharpe P, Alalawi A, Jordan TJ, et al. Low-cost commercial glass beads as dosimeters in radiotherapy. *Radiat Phys Chem* (2014) 97:95–101. doi:10.1016/j.radphyschem.2013.11.007

18. Nabankema SK, Jafari SM, Peet SC, Binny D, Sylvander SR, Crowe SB. Wearable glass beads for *in vivo* dosimetry of total skin electron irradiation treatments. *Radiat Phys Chem* (2017) 140:314–8. doi:10.1016/j.radphyschem.2016.12.013

19. Zschech C, Pech M, Müller MT, Wiessner S, Wagenknecht U, Gohs U. Continuous electron-induced reactive processing - a sustainable reactive processing method for polymers. *Radiat Phys Chem* (2020) 170:108652. doi:10.1016/j.radphyschem.2019.108652

20. Finkensieper J, Mayerle F, Rentería-Solís Z, Fertey J, Makert GR, Lange F, et al. Apicomplexan parasites are attenuated by low-energy electron irradiation in an automated microfluidic system and protect against infection with toxoplasma gondii. *Parasitol Res* (2023) 122:1819–32. doi:10.1007/s00436-023-07880-w

21. Biosciences B. *Multicolor flow cytometry* (2024).

22. H D, W J, K L. Radiation field distributions of an industrial electron beam accelerator. *Front Neurosci* (2000) 161-163:1154–8. doi:10.1016/S0168-583X(99)00811-3

23. Sharpe P, Miller A. *Guidelines for the calibration of routine dosimetry systems for use in radiation processing*. Npl Report CIRM 29 (2009).

24. Brooks SE, Seitzinger NK, Davis LM, Keller RA, Soper SA. Detection of single fluorescent molecules. *Chem Phys Lett* (1990) 174:553–7. doi:10.1016/0009-2614(90)85485-U

25. Wabuyele MB, Ford SM, Stryjewski W, Barrow J, Soper SA. Single molecule detection of double-stranded dna in poly(methylmethacrylate) and polycarbonate microfluidic devices. *Electrophoresis* (2001) 22:3939–48. doi:10.1002/1522-2683(200110)22:18<3939::aid-elps3939>3.0.co;2-9

26. Piruska A, Nikcevic I, Lee SH, Ahn C, Heineman WR, Limbach PA, et al. The autofluorescence of plastic materials and chips measured under laser irradiation. *Lab A Chip* (2005) 5:1348–54. doi:10.1039/b508288a

27. Baldini F, Carloni A, Giannetti A, Porro G, Trono C. An optical pmma biochip based on fluorescence anisotropy: application to c-reactive protein assay. *Sensors Actuators B: Chem* (2009) 139:64–8. doi:10.1016/j.snb.2008.08.027

28. Kry SF, Alvarez P, Cygler JE, DeWerd LA, Howell RM, Meeks S, et al. Aapm tg 191: clinical use of luminescent dosimeters: tlds and oslds. *Med Phys* (2020) 47:e19–e51. doi:10.1002/mp.13839

29. Soares CG, Vynckier S, Järvinen H, Cross WG, Sipilä P, Flühs D, et al. Dosimetry of beta–ray ophthalmic applicators: comparison of different measurement methods. *Med Phys* (2001) 28:1373–84. doi:10.1118/1.1376441

30. Bhatt BC, Kulkarni MS. Thermoluminescent phosphors for radiation dosimetry. *Defect and Diffusion Forum* (2013) 347:179–227. doi:10.4028/www.scientific.net/DDF.347.179